ISIJ International, Vol. 43 (2003), No. 10, pp. 1630–1639

Nucleation of Proeutectoid Ferrite on Complex Precipitates in Austenite

T. FURUHARA, J. YAMAGUCHI,[1] N. SUGITA,[2] G. MIYAMOTO[3] and T. MAKI

Department of Materials Science and Engineering, Kyoto University, Sakyo-ku, Kyoto, 606-8501 Japan.
1) Formerly Graduate Student, Kyoto University, now at Nippon Steel Corp., Nagoya Works, Tokai 851-0392 Japan.
2) Formerly Graduate Student, Kyoto University, now at Hitachi, Ltd., Kodaira Operation, Kodaira, Tokyo 187-8588 Japan.
3) Graduate Student, Kyoto University, Sakyo-ku, Kyoto, 606-8501 Japan.

(*Received on March 12, 2003; accepted in final form on May 9, 2003*)

Effect of various intragranular inclusions or precipitates (MnS, VC and V(C,N)) on the microstructure and kinetics of intragranular ferrite transformation at the temperatures between 973 and 823 K was studied using various Fe–2Mn–(0.13, 0.2)C(mass%) alloys with the small addition of sulfur, vanadium, and nitrogen. In Fe–2Mn–0.13C–50ppmS and Fe–2Mn–0.2C–470ppmS alloys, MnS particles, mostly incoherent in austenite, do not act as effective nucleation sites of ferrite. V addition slightly improves the potency of MnS as ferrite nucleation site by forming MnS+VC complex precipitates. The addition of both V and N largely enhances the intragranular nucleation of ferrite idiomorph on the MnS+V(C,N) complex precipitate. It is considered that two factors, *i.e.*, (1) the advantage in the balance of interphase boundary energy and (2) the increase in the fraction of V(C,N) precipitate by the addition of nitrogen, are mainly responsible for the promotion of intragranular ferrite formation on the MnS+V(C,N) complex precipitate.

KEY WORDS: phase transformation; precipitation; steel; austenite; ferrite; carbide; nitride; sulfide; inclusion; crystallography; interphase boundary.

1. Introduction

The refinement of ferrite+pearlite microstructure is important to improve the mechanical properties of low alloy steels. Intragranular ferrite nucleation on inclusions and precipitates in austenite (fcc γ) has been used to refine the microstructure of steels to improve the toughness in low and medium carbon steels when the deformation of austenite matrix before transformation is hardly applicable[1] such as the heat affected zone formed in welding of structural steels. Among various kinds of inclusions and precipitates, B1(NaCl)-type sulfides, carbides and nitrides are the most promising ones as intragranular ferrite nucleation sites.[2,3]

(MnS+V(C,N)) complex precipitates are currently thought as one of the most superior nucleation sites of intragranular ferrite in medium carbon steel without heat treatment after hot forging.[2] Ishikawa *et al.*[2] reported that the addition of V and N is necessary to promote the intragranular ferrite transformation in an Fe–1.5Mn–0.25C based steel during continuous cooling. They proposed that the nucleation rate of ferrite is larger at such complex precipitates because of a lower energy of ferrite/V(C,N) boundary. Qiu and Nagumo[4–6] studied the ferrite transformation kinetics at austenite grain boundaries, which are the most competitive nucleation site of ferrite for intragranular inclusion/precipitate, in V–N added Fe–1.5Mn–0.25C based alloys. They reported that the addition of V and N results in the decrease in the growth rate of grain boundary ferrite.[5,6] Ohmori *et al.*[7] studied the nucleation kinetics of intergranular and intragranular ferrite in V-added Fe–1.5Mn–0.15C alloys with low and high nitrogen contents. They showed that the addition of V and N increases the nucleation rate of grain boundary ferrite. In their alloys, S content is much lower than the alloys studied by Ishikawa *et al.*, leading to no significant effect of V–N addition on intragranular ferrite kinetics. These studies indicate that the presence of MnS should play important roles in intragranular ferrite transformation kinetics. Recently, some of the present authors reported an acceleration of pearlite transformation by the formation of MnS+VC complex precipitates in Fe–12Mn–0.8C alloys with V addition.[8] However, there was no systematic study that examined the potency of inclusions as the nucleation site of ferrite in terms of the amount of MnS and V(C,N) during isothermal ferrite transformation.

The present study aims to reveal the effect of MnS and V(C,N) on the microstructure and kinetics of proeutectoid ferrite transformation in Fe–2Mn–0.2C alloys with various S, V and N contents. Special attention is paid to the potency of MnS+V(C,N) complex precipitates as nucleation sites of intragranular ferrite.

2. Experimental Procedure

Table 1 shows the chemical compositions of Fe–2Mn–(0.13, 0.2)C hypoeutectoid steels with various alloying elements. In Steel A containing only 7 ppm of S, MnS is hardly formed. In Steel B with 50 ppm of S and Steel C with 470 ppm of S, different amounts of MnS are formed. Steels D and E, with the S content nearly the same as Steel C,

Table 1. Chemical compositions of the materials used (mass%).

	C	Mn	S	V	N	Fe
Steel A	0.21	2.0	0.0007	——	——	bal.
Steel B	0.13	1.9	0.005	——	0.0009	bal.
Steel C	0.20	2.0	0.047	0.01	0.0019	bal.
Steel D	0.20	2.1	0.054	0.31	0.0027	bal.
Steel E	0.20	2.0	0.047	0.30	0.0114	bal.

contain similar dispersion of MnS as that of Steel C. In Steel D, VC precipitates in austenite with the addition of 0.3 mass% V. V(C,N) precipitation occurs in Steel E due to the addition of both V and N. The solution temperatures of inclusion/precipitate phases in austenite were calculated by using the solubility product equation proposed by Turkdogan[9] for MnS and Thermo–Calc for VC and V(C,N).

Figure 1 shows the heat treatments employed in the present study. Austenitizing was made at 1 473 K for 0.6 ks after homogenizing at 1 473 K for 43.2 ks of hot-rolled plates. The average grain sizes of austenite after this treatment were 520 μm for Steel A, 450 μm for Steel B, and nearly equal to 150 μm for all of Steels C–E. After austenitizing at 1 473 K, the precipitation treatments of VC and V(C,N) at 1 173 K for various periods were performed for Steels D and E, followed by isothermal holding in the temperature range between 973 and 823 K to promote proeutectoid ferrite transformation.

Microstructures of the transformed specimens were observed by means of optical, scanning and transmission electron microscopy (SEM and TEM). Volume fractions of ferrite were determined by point counting in optical micrographs. Electron probe microanalyzer (EPMA) and TEM-EDS (energy dispersive X-ray spectroscopy) analyses were made for identifying precipitate phases which act as ferrite nucleation sites. For optical and SEM observations, specimens were etched with 5 % nital. TEM thin foil specimens, 3 mm in diameter, were prepared by mechanical thinning followed by Argon ion thinning. TEM observation was performed by using Joel JEM-200CX and Philips CM200, CM200FEG operated at 200 kV.

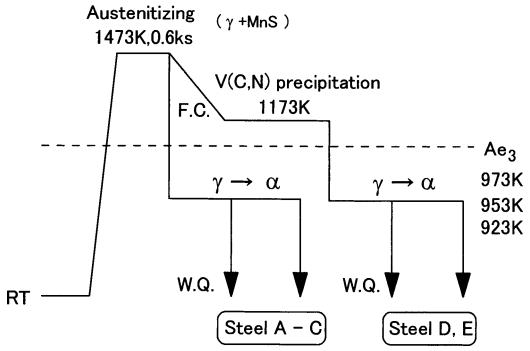

Fig. 1. The heat treatments employed in the present study

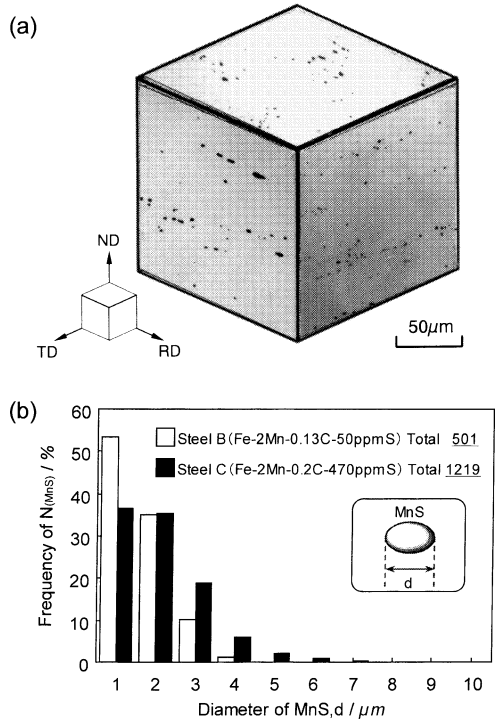

Fig. 2. The distribution of MnS in the materials; (a) the optical micrograph of hot rolled plates in Steel C (3-dimentionl view), (b) size distribution of MnS particles in Steels B and C.

3. Results

3.1. Effect of MnS on Intragranular Ferrite Transformation

Figure 2(a) shows the optical microstructure of the specimen water-quenched after austenitizing in Steel C containing 470 ppm of S. Because the specimens were hot-rolled, MnS particles are aligned roughly parallel to the rolling plane. Figure 2(b) shows the size distribution of MnS in Steels B and C measured by optical microscope. The number of MnS particles is less in Steel B because the amount of S content is smaller. Although diameters of MnS are mostly smaller than 3 μm in both steels, the number of larger particles is smaller in Steel B with less S content than Steel C. The size distributions of MnS particles in Steels D and E were nearly the same as that in Steel C. MnS particles much smaller than 1 μm in diameter are perhaps not included in the measurement due to lack of resolution. However, it should be noted that such a small MnS were hardly recognized in TEM observation of Steel E of which S content is nearly the same as Steel C.

Figures 3(a) to 3(c) show the optical microstructures of Steels A to C, respectively, transformed at 953 K for 3.6 ks after austenitizing at 1 473 K. At this austenitizing temperature, most of MnS particles do not dissolve into austenite in Steels B and C and thus the intragranular nucleation sites of ferrite are the MnS particles incoherent with respect to austenite. With increasing S content, the fraction of ferrite transformed increases due to the decrease in austenite grain size under the pinning effect of MnS. Most of ferrites are formed at γ grain boundaries at 953 K although small amounts of intragranular ferrite are observed in Steels B and C (*e.g.*, see the arrows in Fig. 3(c)). Most of ferrites were idiomorphic but some intragranular ferrites exhibit Widmanstätten morphology implying that there is a large scattering in the orientation relationship between intragranular ferrite and austenite. As shown in the later section, by lowering transformation temperature further, a potency of MnS as ferrite nucleation site is increased slightly.

It was reported that Mn-depleted zone around MnS is important to promote intragranular ferrite transformation in heat-affected zone of structural steels.[10–12] In the present study, the austenitizing at 1 623 K for 1.8 ks was also employed before isothermal holding for ferrite transformation. Even though the austenite grain size slightly increased from 155 to 170 μm by raising the austenitizing temperature, there was no change in the effect of MnS as intragranular ferrite nucleation site. The amount of S which is dissolved at 1 623 K is still about a few percents of the total S content. It is thought that austenitizing at much higher temperature is necessary to promote the ferrite nucleation at MnS in Steels B and C to produce a large Mn-depleted zone by dissolving a more amount of MnS.

3.2. Effect of V and N Addition on Intragranular Ferrite Transformation

Figures 4(a) to 4(c) show the optical microstructures of Steels C, D and E transformed at 953 K for 0.6 ks, respectively. The V(C,N) precipitation treatment at 1 173 K for 3.6 ks was performed for Steels D and E before ferrite transformation. By adding 0.3 mass% of V, intragranular ferrite transformation is promoted in some degree in Steel D (Fig. 4(b)) than in Steel C (Fig. 4(a)). The addition of both V and N clearly enhances the intragranular ferrite transformation in Steel E (Fig. 4(c)). Figure 4(d) shows the volume fraction of ferrite transformed at 953 K for 0.6 and 1.8 ks. Nucleation at austenite grain boundaries is still dominant in ferrite transformation in all of those steels. For Steel C (with MnS), the fraction of intragranular ferrite is small. In Steel D (with MnS+VC), the ferrite transformation kinetics at 953 K is remarkably slower than that in Steel C. The fraction of intragranular ferrite is also low in this alloy. However, it seems to be increasing as transformation time becomes longer. On the other hand, Steel E (with MnS+V(C,N)) contains a much higher fraction of intragranular ferrite than Steels C and D.

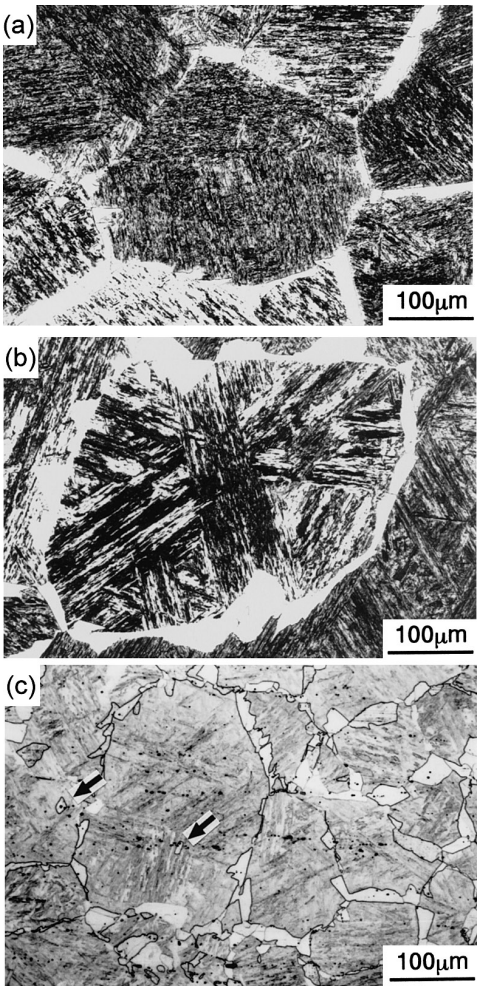

Fig. 3. Optical microstructure of the specimens with MnS transformed at 953 K for 3.6 ks; (a) Steel A (7 ppm S), (b) Steel B (50 ppm S) and (c) Steel C (470 ppmS).

Figure 5 shows the EPMA analysis of the complex precipitate which acts as a nucleation site of intragranular ferrite in Steel D. Figure 5(a) shows the scanning electron micrograph of a typical intragranular ferrite. The X-ray spectrum of Fig. 5(b) shows that the large particle ((b) in Fig. 5(a)) on which ferrite nucleated is MnS. The X-ray spectrum (Fig. 5(c)) taken from the bright particle ((c) in Fig. 5(a)) at the MnS/ferrite boundary shows that the particle contains V. Thus, it is concluded that the ferrite nucleated at VC formed on MnS. **Figure 6** shows the EDS analysis of an intragranular ferrite on a complex precipitates in Steel E. The spectrum of Fig. 6(b) was taken from ferrite in the micrograph of Fig. 6(a). The spectrum of Fig. 6(c) shows the large particle with a spherical boundary is MnS and that in 6(d) revealed that a facetted precipitate on MnS is V(C,N). Analysis of the selected area diffraction patterns taken from those precipitates also confirmed the identification of those phases by EDS.

Figure 7(a) shows the fractions of MnS particles which act as intragranular ferrite nucleation sites in the specimens of Steels C, D and E transformed at 953 K for 0.6 ks. In the case that multiple MnS particles are contained in a single intragranular ferrite, the largest particle was chosen as the nucleation site of ferrite. Nearly 20% of MnS particles become the nucleation sites of ferrite when V(C,N) precipitates are formed by the aging at 1 173 K. Figure 7(b) is the

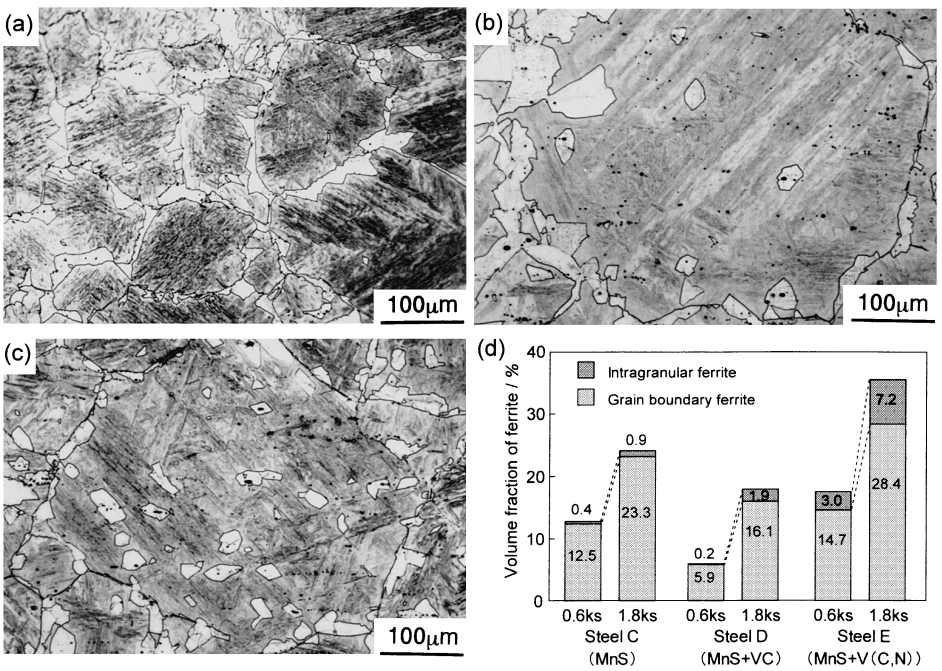

Fig. 4. Optical microstructure of the specimens transformed at 953 K for 0.6 ks; (a) Steel C (with MnS), (b) Steel D (with MnS+VC), (c) Steel E (with MnS+V(C,N)), (d) the volume fractions of ferrite in Steels C to E transformed at 953 K for 0.6 and 1.8 ks. For Steels D and E, the aging treatment was performed at 1 173 K for 3.6 ks prior to ferrite transformation.

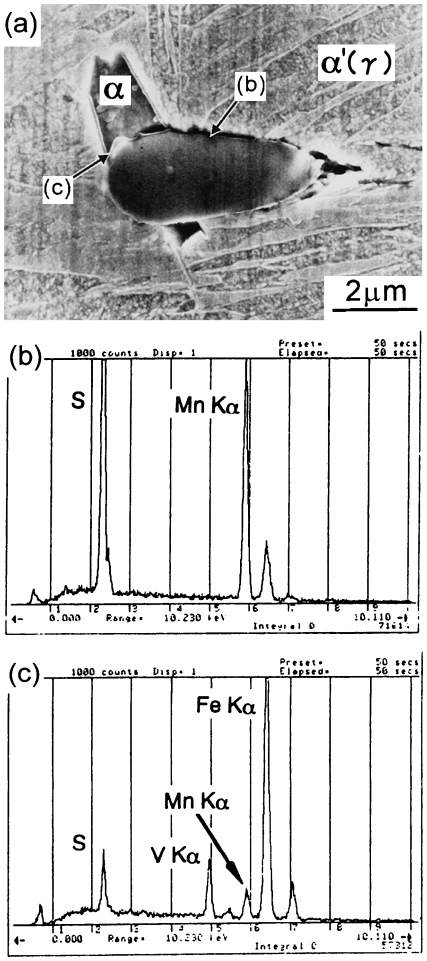

Fig. 5. The result of EPMA measurement of intragranular ferrite in Steel D (953 K, 1.8 ks transformed); (a) scanning electron micrograph and X-ray spectra from (b) MnS and (c) VC.

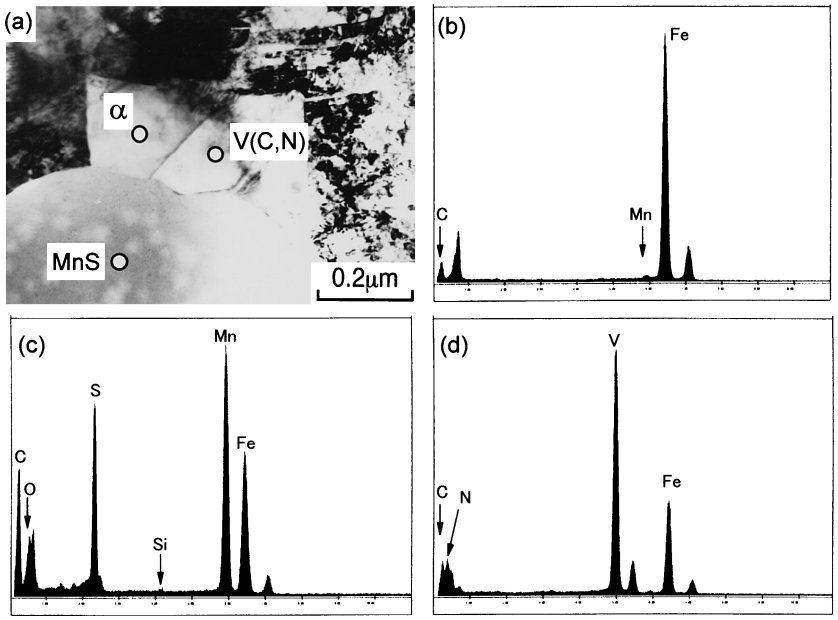

Fig. 6. The result of TEM-EDS measurement of intragranular ferrite in Steel E (953 K, 0.6 ks transformed); (a) the bright field micrograph and X-ray spectra from (b) ferrite, (c) MnS and (d) V(C,N).

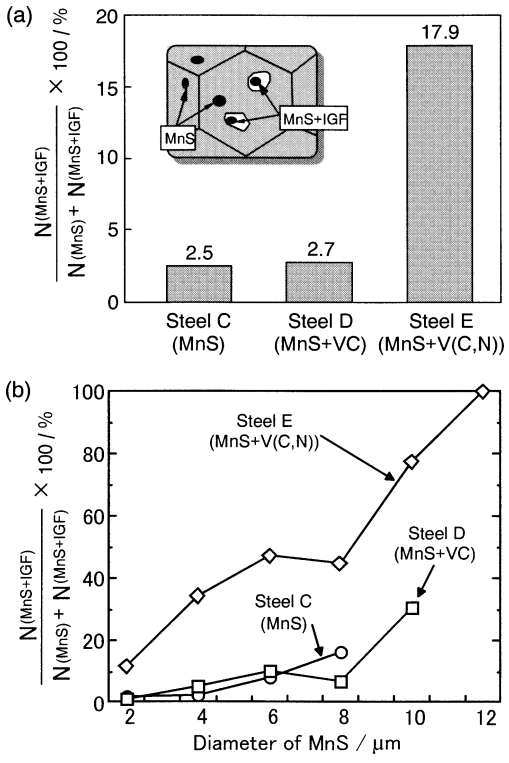

Fig. 7. (a) Fraction of the MnS (with VC or V(C,N)) acting as intragranular ferrite nucleation sites with respect to the total numbers of MnS inclusions observed in optical microscope (953 K, 0.6 ks transformed), (b) fraction of the MnS with intragranular ferrite plotted against the diameter of MnS. For Steels D and E, the aging treatment was performed at 1 173 K for 3.6 ks prior to ferrite transformation.

fraction of MnS acting as ferrite nucleation site plotted against the diameter of MnS. For all the size of MnS, the potency of MnS as nucleation site is increased with V(C,N) precipitation. Since the smaller MnS, which is much larger in particle density, is more active as ferrite nucleation sites in Steel E, the density of intragranular ferrite is larger in this alloy than in Steels C and D. It should be noted, however, that some of those MnS particles can be embedded by the ferrite which grew from the other particles not locating on the polished plane.

The potency of those complex precipitates as the nucleation site for intragranular ferrite changes depending on transformation temperature of ferrite. **Figures 8**(a) to 8(d) show the optical microstructures of Steel E transformed at different temperatures after the aging at 1 173 K for 3.6 ks. At 973 K (Fig. 8(a)), intragranular ferrite is hardly observed, indicating that the MnS+V(C,N) complex precipitate is less potent as a ferrite nucleation site than the austenite grain boundary. As transformation temperature is lowered, MnS+V(C,N) precipitates become more active as nucleation sites of idiomorphic ferrite, as are seen in Figs. 8(b) (953 K) and 8(c) (873 K). This might be due to the increase in the amount of V(C,N) precipitating on MnS during the cooling from 1 173 K and the isothermal holding at a lower transformation temperature. When the transformation temperature is lowered to 823 K, the morphology of ferrite changes to acicular from idiomorphic (Fig. 8(d)) as previously reported.[13] This implies that, when supercooling is large, ferrite prefers to hold coherency with the austenite matrix rather than the V(C,N) where it nucleated. **Figure 9** shows the volume fractions of ferrite in Steels C and E transformed at 873 K where idiomorphic ferrite forms. Even the MnS particle without V(C,N) in Steel C becomes

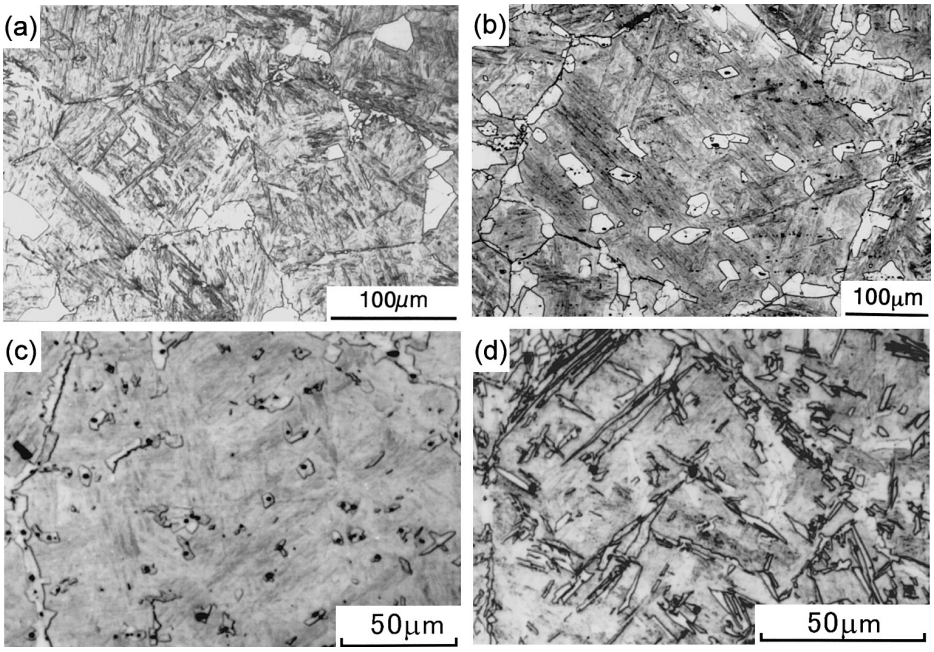

Fig. 8. Optical microstructures of the Steel E aged at 1 173 K for 3.6 ks and transformed at different temperatures; (a) 973 K for 3.6 ks, (b) 953 K for 0.6 ks, (c) 873 K for 60 s, (d) 823 K for 20 s.

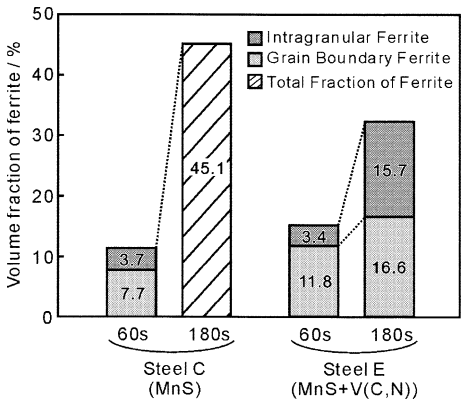

Fig. 9. Volume fractions of ferrite transformed at 873 K for 60 s and 180 s in Steels C (with MnS) and E (with MnS+V(C,N)).

a little more active at this transformation temperature as the ferrite nucleation site. However, as transformation proceeds, Widmanstätten ferrite sideplates grow from grain boundary ferrite allotriomorphs. On the other hand, in the case of Steel E, the formation of sideplates is suppressed and many intragranular ferrite idiomorphs are formed on the MnS+V(C,N) complex precipitates, leading to a higher fraction of intragranular ferrite.

Figure 10 shows the effect of aging periods at 1 173 K for V(C,N) precipitation on the subsequent ferrite transformation kinetics in Steel E. V(C,N) precipitation affects differently the ferrite kinetics depending upon the aging condition. When no aging was performed before transformation, only a small fraction of intragranular ferrite is formed in the early stage (Fig. 10(a)). As the transformation proceeds, intragranular ferrite formation occurs a little more frequently. In the specimen aged for 3.6 ks, the fraction of intragranular ferrite is larger than in the cases without aging. After a prolonged aging for 86.4 ks, ferrite transformation kinetics is clearly accelerated. However, the fraction of intragranular ferrite is smaller than that in the specimens aged at 3.6 ks due to the relative increase of grain boundary ferrite.

Crystallographic orientation relationships between MnS+V(C,N), austenite and ferrite were studied by Kikuchi pattern analysis as reported preliminarily.[13] More detailed report will be made elsewhere.[14] **Figure 11** summarizes the ferrite/(MnS+V(C,N))/austenite three-phase crystallographic relationship for intragranular ferrite idiomorph. Since MnS contained in the alloy such as Steels D and E cannot be dissolved into austenite even at very high temperature, MnS particles remain incoherent with respect to the austenite matrix without specific orientation relationships after austenitizing at 1 473 K. V(C,N), which holds a cube–cube orientation relationship ($\langle 001\rangle_\gamma // \langle 001\rangle_{V(C,N)}$) when they forms within austenite grains,[15] does not exhibit any specific orientation relationship with respect to austenite matrix. This implies that the V(C,N)/austenite interphase boundary which acts as ferrite (mostly idiomorphic) nucleation sites has a less coherent structure. Between ferrite and V(C,N), there are often Baker–Nutting (B–N) orientation relationship[16] ($(001)_\alpha // (001)_{V(C,N)}$, $[110]_\alpha // [100]_{V(C,N)}$), as Ishikawa *et al.*[2] reported. However, other, apparently not specific, orientation relationships were also observed between these phases.[13] For such non-specific orientation relationships, some kinds of near-parallel relationships between low-indexed planes or directions were recognized. Because such low-energy ferrite/V(C,N) orientation relationships exist, the ferrite/austenite orientation relationship turn to be non-specific, which might result in smaller anisotropy of ferrite/austenite interphase boundary energy. Those crystallographic analyses revealed that the random matrix/precipitate orientation relationships are obtained for the nucleation at incoherent interphase boundaries. When the driving force for ferrite transformation is increased by lowering transformation temperature, acicular ferrite becomes dominant as shown in Fig. 8(d) holding near K–S relationships with respect to austenite.[13] This implies that, when supercooling is large, ferrite prefers to hold coherency with the austenite matrix rather than the V(C,N) where it nucleated.

4. Discussion

In the present study, it was found that MnS is not so active as the nucleation site of ferrite in the austenite grain. A

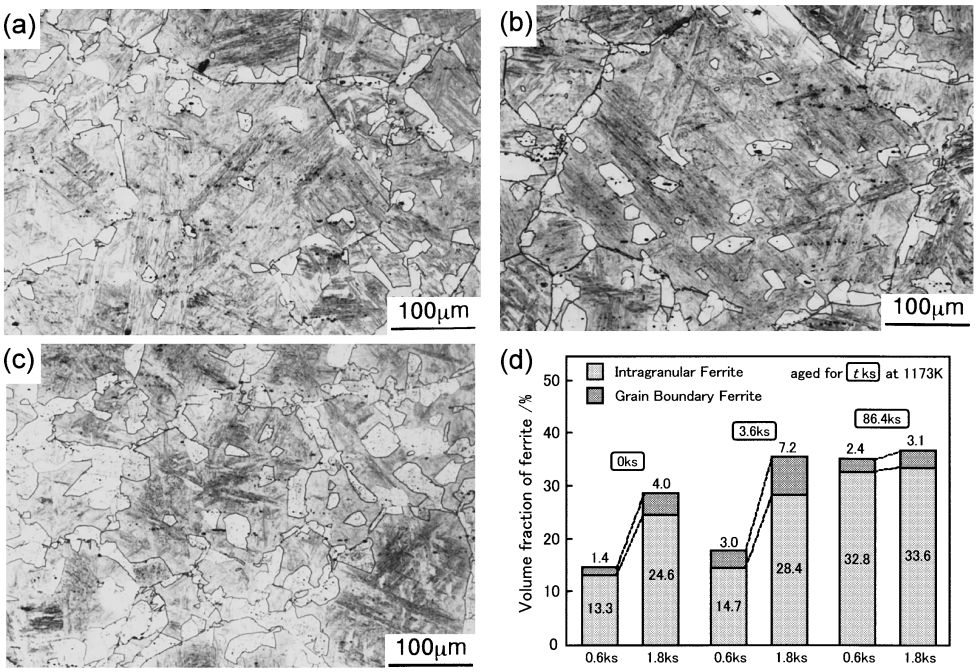

Fig. 10. Optical microstructures of the Steel E aged at 1 173 K for various periods and transformed at 953 K for 0.6 ks; (a) without aging; (b) aged for 3.6 ks and (c) 86.4 ks, (d) the volume fraction of ferrite transformed at 953 K for 0.6 and 1.8 ks in different aging conditions.

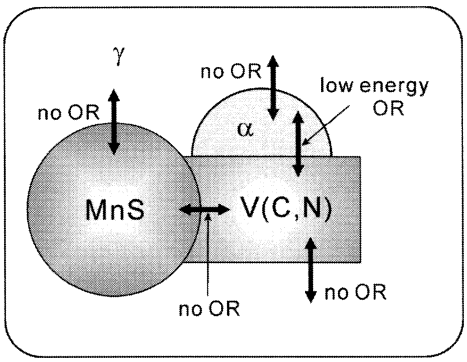

Fig. 11. Schematic illustration of the crystallographic relationship between ferrite, MnS+V(C,N) complex precipitate and austenite in Steel E.

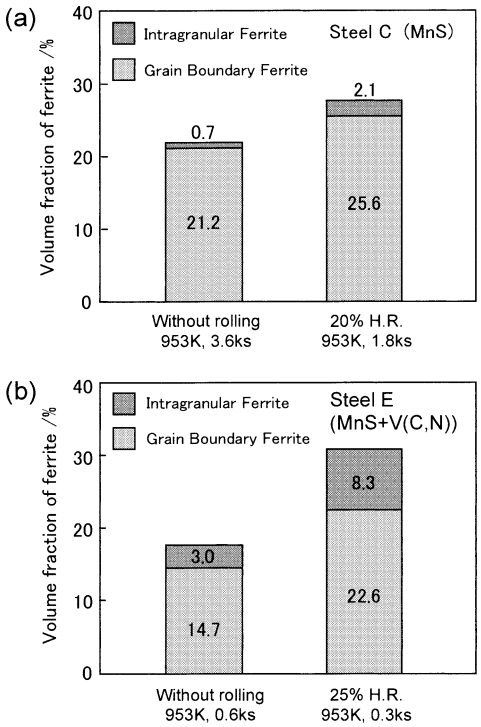

Fig. 12. Volume fractions of ferrite transformed at 953 K after hot rolling at 1 173 K; (a) Steel C (rolled by 20 %) and (b) Steel E (aged at 1 173 K for 3.6 ks and rolled by 25 %).

slight increase of intragranular ferrite was observed when MnS+VC complex precipitates were formed by the addition of V. The addition of both V and N effectively promoted intragranular ferrite transformation by forming MnS+V(C,N) complex precipitates. As summarized previously,[17,18] three factors are considered to affect the intragranular ferrite nucleation at inclusions (substrate) in austenite; (1) the energy balance of interphase boundaries between the three phases (ferrite, substrate and austenite), (2) the inhomogeneity in chemical composition near the substrate (*e.g.*, Mn depleted zone around MnS), (3) the strain field around inclusion/precipitate formed during cooling due to the difference in thermal expansion between inclusion and austenite. In the present section, the difference in potency as ferrite nucleation site for those precipitates is discussed based on these factors.

4.1. Effect of Strain Field around Inclusion/Precipitate in Austenite Matrix

The elastic stress associated with the difference in thermal contraction between austenite and inclusion (the factor (3)) can be important. The expansion coefficient of VC or VN is smaller than MnS so that a larger stress effect can be expected for VC and V(C,N) as discussed previously.[8,17] However, such elastic stresses are so large that plastic accommodation should take place in austenite by forming dislocations around the inclusion or precipitate.[17,18] Thus, in the present study, slight hot deformation of austenite was performed before ferrite transformation in order to study the effect of dislocations on the intragranular ferrite transformation in the specimen containing complex precipitate. **Figures 12**(a) and 12(b) show the effect of 20–25 % hot rolling of austenite at 1 173 K on the ferrite transformation kinetics at 953 K in Steels C (MnS) and E (MnS+V(C,N)). At this transformation temperature, idiomorphic ferrites are formed as shown in Figs. 7 and 8. By a small amount of hot deformation, both of grain boundary and intragranular fer-

rite nucleation kinetics are accelerated. However, the enhancement of ferrite transformation by hot deformation in Steel C is small. This implies that plastic accommodation in austenite itself does not promote intragranular ferrite transformation significantly. Since it is known that deformation bands as well as deformed annealing twin boundaries act as preferential nucleation sites within the austenite grain,[19,20] the increase in ferrite nucleation at MnS by hot rolling should be less than the observed increase in intragranular ferrite in Fig. 12(a). In Steel E, a relatively large increase in each of grain boundary and intragranular ferrite volume fractions is seen (Fig. 12(b)). Similar effects of austenite deformation were recognized by the present authors in similar low-carbon, low-alloy steels.[21] The possible reason for this enhancement is that the deformation of austenite causes the rapid increase in V(C,N) precipitation during the cooling from the deformation temperature (1 173 K) to the ferrite transformation temperature (953 K).

As supercooling is increased, acicular ferrite becomes dominant in intragranular ferrite morphology (Fig. 8(d)). For the acicular ferrite holding near K–S orientation relationships with austenite,[13,22] transformation strain contains a shear component due to stacking change from fcc to bcc. Such a strain can be accommodated effectively by the strain field of dislocations so that plastic deformation around inclusion/precipitate might play a more important role for acicular ferrite formation. Additionally, the size of ferrite nucleus should become smaller as supercooling becomes larger. Since the strain energy density around the dislocation drastically increases as approaching to the dislocation core, ferrite nucleation on the dislocation can be more favored by lowering transformation temperature, as previously discussed for the cementite precipitation in an Al-killed ultra-low carbon steel.[23]

4.2. Effect of Inhomogeneous Distribution of Alloying Element

For the inhomogeneity of alloying element (the factor (2)), Mn depleted zone around MnS was pointed out previously as a major factor to promote intragranular ferrite nucleation.[10] The presence of Mn depleted zone was recently confirmed by TEM-EDS measurements.[11,12] In the present study, the austenitizing of Steel C at 1 623 K did not promote intragranular ferrite transformation. Only a few percents of the total S content (470 ppm) in Steel C would be dissolved in austenite by this treatment. Although the local equilibrium calculation assuming the iso-activity condition for S[24] estimates the depletion of about 2 mass% Mn, leading to the increase in Ae_3 temperature for paraferrite transformation by 100 K. This might indicate that Mn depleted zone formed around MnS in the present treatment is not large enough to promote intragranular ferrite transformation since only a small amount of MnS is dissolved.

The precipitation of V(C,N) could induce inhomogeneity of carbon although such a possibility was denied by the previous discussion based on diffusion field formed during the growth of V(C,N).[2] However, Han *et al.*[25] reported the formation of abnormal ferrite at austenite grain boundaries in an Fe–Mn–C–V hypereutectoid alloy. They proposed that the non-equilibrium C-depleted zone around VC precipitated at the austenite grain boundary promotes the formation of such a ferrite in spite that the nominal composition should result in proeutectoid cementite precipitation. The present authors proposed a similar mechanism for the formation of intragranular pearlite on MnS+VC complex precipitates in an Fe–Mn–C–V alloy,[8] of which composition is about the same as that of Han *et al.* The complex transformation behavior with aging time at 1 173 K seen in Fig. 10 implies that non-equilibrium precipitation of V(C,N) affects strongly the kinetics of intragranular ferrite transformation as in the case of intragranular pearlite formation on the complex precipitate.

4.3. Effect of Interphase Boundary Energy Balance

It is necessary for the estimation of interphase boundary energy between austenite/precipitate/ferrite (the factor (1)) to characterize the crystallographic feature (such as orientation relationship, habit plane) of those phases. The present authors determined the crystallographic features of B1-type precipitates formed in austenite.[15] VC and TiC are formed with a cube–cube orientation relationship ($\langle 001\rangle_\gamma // \langle 001\rangle_p$) whereas MnS holds the cube-on-edge relationship ($(001)_\gamma // (001)_{MnS}$, $[100]_\gamma // [110]_{MnS}$). The orientation relationship between precipitates and their austenite matrices were explained reasonably well by the minimization of misfit strain. The interphase boundary between matrix and precipitate is supposed to be coherent in the nucleation stage and should turn to be semi-coherent in order to reduce the strain energy. The equilibrium shape of precipitate can be determined by minimization of total interfacial energy when strain is accommodated. Turnbull[26] proposed that the total energy of a semi-coherent boundary is approximately the sum of the chemical component (originated from the difference of chemical bonding between the matrix and product phases) and the structural component (originated from the self and interaction energy of misfit dislocations). In this section, the interphase boundary energy between austenite, B1-type carbides, nitrides (or sulfides) and ferrite was estimated to discuss the potency of B1-type precipitates as the nucleation sites in the proeutectoid ferrite reaction.

Several attempts to estimate bond energies for B1-type precipitates have been made.[27–31] Cottrell[27,28] developed the model for bond energy calculation to estimate the cohesive energy of B1-type carbides. According to him, the M–C bond is attractive and the M–M and C–C bonds are both repulsive. The magnitude of bond energy is largest for the M–C bond in the carbide. The numbers of M–C bonds formed per unit area is largest for the $\{001\}_\gamma$ surface, as shown in Table A1 where M–N and M–C bonds are represented as M–X. These considerations lead to the deduction that the interphase boundary energy of B1-type carbide is presumably the lowest for the $\{001\}_\gamma$. Recently, the discrete lattice model, originally applied in disordered fcc/fcc boundaries, were extended for the calculation of the chemical interphase boundary energy between B1-type precipitate and fcc matrix (austenite) being related with the cube–cube orientation relationship.[29] It was shown that the lowest energy facet is indeed the $\{001\}_\gamma // \{001\}_p$ for the cube–cube orientation relationship and the boundary energy was higher for nitrides than carbides because of higher cohesive energy. However, the present authors showed that VC or TiC exhibit only the $\{111\}_\gamma$ facets in the early stage of aging and the $\{001\}_\gamma$ facets were observed only after prolonged aging.[32] Such an observation indicates that higher energy facets can be formed by some kinetic effects.

Interphase boundary energy between ferrite and B1-type precipitate plays an important role in the nucleation kinetics of intragranular ferrite. It was considered that the austenite/V(C,N) boundary of which habit plane is $(001)_\alpha // (001)_{B1}$ is a superior nucleation site because of good coherency across this boundary for the B–N orientation relationship.[2] The comparison of structure components was

made for both of austenite/precipitate and ferrite/precipitate boundaries, which has led to the similar deduction.[17] Zhang *et al.*[30] estimated the chemical component on the $(001)_{\alpha}//(001)_{B1}$ boundaries for the B–N relationship by a Lenerd–Jones model. According to them, VN has lower boundary energy than TiO, TiN and TiC with respect to ferrite and the chemical component of interphase boundary energy is often larger than the structural component. Most recently, a more systematic calculation was made for ferrite/B1-type precipitate interphase boundary energies by the discrete lattice model. It was shown that the boundary energy was higher for nitrides than carbides as in austenite.[31] However, the reason for larger promotion of ferrite nucleation by B1-type carbides and nitrides than MnS is still not understood.

In the present study, the bond energy between each element was estimated from the interaction parameters in the Hillert–Staffansson sub-regular solution model (HSM).[33] For a given boundary, the chemical component of the interphase boundary energy was calculated by counting the numbers of bonds broken and formed, following to the nearest-neighbor broken-bonding model.[34] Also, the structural component of interphase boundary energy was estimated using the equation by van der Merwe *et al.*[35] by following the previous examination.[17] Both methods are described in Appendices I and II. **Table 2** shows the calculated values of both components of interphase boundary energy between austenite (or ferrite) and B1-type precipitates at 950 K. In the present calculation, chemical component for VC, VN, both of $\{100\}_{\gamma}$ and $\{111\}_{\gamma}$ facets are considered whereas interphase boundary energy for the $\{001\}_{\gamma}//\{001\}_{B1}$ facet was calculated for MnS. For simplicity, it was assumed that some specific orientation relationships are held across the ferrite/precipitate and austenite/precipitate interphase boundaries (see Appendix II) although it was observed that the actual orientation relationship is non-specific in general.

The chemical components for VN/austenite or VN/ferrite interphase boundaries are larger than those for VC/austenite or VC/ferrite boundaries in a qualitative agreement with the previous studies.[29,31] Contrarily, the structural components are nearly the same for VC and VN. The $(001)_{V(C,N)}$ boundary in ferrite has a significantly smaller structural energy, with the B–N orientation relationship, than the $(111)_{V(C,N)}$ boundary in ferrite whereas the ones for the $(001)_{V(C,N)}$ and $(111)_{V(C,N)}$ boundaries in austenite are nearly the same. Because of this energetic advantage, it is expected that the $(001)_{V(C,N)}$ boundary with the B–N relationship is a more preferred ferrite nucleation site than the $(111)_{V(C,N)}$ boundary for the same ferrite/austenite interphase boundary energy. On the other hand, the $(001)_{MnS}$ boundary should not be an effective nucleation site since the interphase boundary energy increases by austenite to ferrite transformation. Thus, it is concluded that the interphase boundary plays an important role on the acceleration of intragranular ferrite transformation by V(C,N) precipitation.

4.4. Effect of N Addition on V(C,N) Precipitation

In the calculation made above, however, there is no significant difference in the interphase boundary energies for VC and VN. Thus, it is thought that boundary energy is not responsible for the larger acceleration of intragranular ferrite formation by V(C,N) precipitation than VC. A possible reason for such acceleration could be the difference in the volume fraction of V(C,N) formed in austenite. **Figure 13** shows the change in volume fractions of V(C,N) and VC in austenite with aging temperature. The addition of 100 ppm N in Steel E drastically increases the equilibrium fraction of V(C,N) in austenite at higher aging temperatures. Thus, the density of V(C,N) on MnS as nucleation site would be larger in Steel E than in Steel D, resulting in the more extensive intragranular ferrite formation in Steel E. However, further study is needed for V(C,N) precipitation kinetics as well as local composition change in austenite during growth of those precipitates to clarify this effect.

Table 2. Austenite/precipitate and ferrite/precipitate interphase boundary energies estimated at 950 K.

Interface	chemical (J/m^2)	structural (J/m^2)	total (J/m^2)
VC(001)/γ	0.398	1.525	1.923
VC(111)/γ	0.982	1.616	2.598
VN(001)/γ	1.940	1.505	3.445
VN(111)/γ	3.606	1.595	5.201
MnS(001)/γ	0.151	0.561	0.712
VC(001)/α	0.145	0.487	0.632
VC(111)/α	2.238	1.301	3.539
VN(001)/α	1.217	0.355	1.572
VN(111)/α	3.865	1.220	5.085
MnS(001)/α	0.247	0.777	1.024

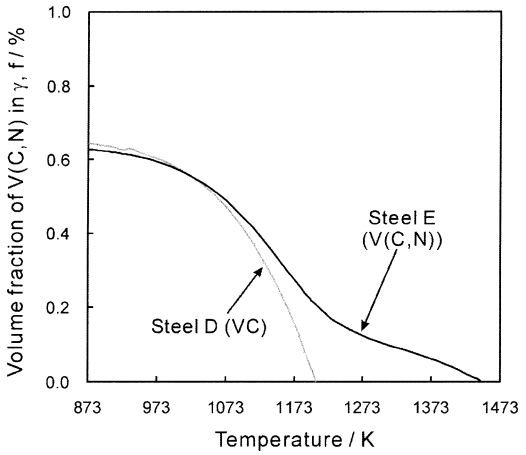

Fig. 13. Change in the equilibrium volume fraction of V(C,N) in austenite with aging temperature, estimated for the Steels D and E by Thermo-calc calculation.

5. Conclusions

The microstructure and kinetics of intragranular ferrite transformation were studied in Fe–2Mn–C alloys with the addition of S, V, and N.

(1) In Fe–2Mn–0.13C–50ppmS and Fe–2Mn–0.2C–470ppmS, MnS which is incoherent in austenite is not so effective as the ferrite nucleation site. V addition slightly improves the potency of MnS as ferrite nucleation site by forming (MnS+VC) complex precipitates.

(2) The addition of both V and N largely promotes the intragranular ferrite nucleation on the (MnS+V(C,N)) complex precipitates. As the size of MnS is larger, the potency of complex precipitates as the ferrite nucleation sites is greater. When the transformation temperature is lower, more intragranular ferrites form at the complex precipitates. When the V(C,N) precipitation treatment was prolonged, intragranular ferrite transformation becomes less active at 953 K, indicating that the non-equilibrium precipitation of V(C,N) is preferred for the promotion of intragranular ferrite transformation.

(3) The chemical component of the interphase boundary energy between austenite (or ferrite) and B1-type precipitate (VC, VN or MnS) was calculated by using thermodynamic parameters under the specific orientation relationship and habit plane. VC or VN has low interfacial energy with respect to ferrite but relatively high interfacial energy with respect to austenite for the $(001)_{V(C,N)}$ boundary compared with MnS. Such advantages of VC and VN over MnS in the balance of interphase boundary energy presumably promote the intragranular ferrite transformation for the complex precipitates. Furthermore, the addition of N with V should increase the amount of V(C,N) precipitate, leading to a larger acceleration on the intragranular ferrite formation than the addition of only V.

Acknowledgments

The financial supports of the Iron and Steel Institute of Japan and the Ministry of Education, Science and Culture through a Grant-in-Aid for Scientific Research (A) No. 08555163 (1998-2000) are gratefully acknowledged.

REFERENCES

1) J. Takamura and S. Mizoguchi: Proc. 6th Int. Iron & Steel Cong., ISIJ, Tokyo, (1990), 591.
2) F. Ishikawa, T. Takahashi and T. Ochi: *Metall. Mater. Trans. A*, **25A** (1994), 929.
3) K. Yamamoto, T. Hasegawa and J. Takamura: *ISIJ Int.*, **36** (1996), 80.
4) P. Qiu and M. Nagumo: *Tetsu-to-Hagané*, **84** (1998), 375.
5) P. Qiu and M. Nagumo: *Tetsu-to-Hagané*, **84** (1998), 592.
6) P. Qiu and M. Nagumo: *Tetsu-to-Hagané*, **85** (1999), 45.
7) A. Ohmori, K. Oi, F. Kawabata and K. Amano: *Tetsu-to-Hagané*, **84** (1998), 797.
8) Z. Guo, N. Kimura T. Furuhara and T. Maki: *ISIJ Int.*, **42** (2002), 1033.
9) E. T. Turkdogan, S. Ignatowicz and J. Pearson: *J. Iron Steel Inst.*, **180** (1955), 349.
10) Y. Ueshima, H. Yuyama, S. Mizoguchi and H. Kajioka: *Tetsu-to-Hagané*, **75** (1989), 501.
11) H. Mabuchi, R. Uemori and M. Fujioka: *ISIJ Int.*, **36** (1996), 1406.
12) G. Shigesato, M. Sugiyama, S. Aihara, R. Uemori and Y. Tomita: *Tetsu-to-Hagané*, **87** (2001), 93.
13) G. Miyamoto, T. Shinyoshi, J. Yamaguchi, T. Furuhara, T. Maki and R. Uemori: *Scr. Mater.*, **48** (2003), 371.
14) T. Furuhara, N. Sugita, N. Kimura, J. Yamaguchi, N. Takemura, T. Shinyoshi, G. Miyamoto and T. Maki: *ISIJ Int.*, **43** (2003), in print.
15) T. Furuhara, N. Sugita and T. Maki: Proc. of 8th Int. Conf. on Intragranular and Interphase Boundaries in Materials, ed. by Y. Ishida *et al.*, JIM, Sendai, (1996), 363.
16) R. G. Baker and J. Nutting: *J. Iron Steel Inst.*, **192** (1959), 257.
17) The Report of Basic Research Committee, Use of Fine Inclusions in Microstructure Control of Steels, ISIJ, Tokyo, (1995), 75.
18) M. Enomoto: *Met. Mater.*, **4** (1998), 115.
19) H. Inagaki: *Trans Iron Steel Inst. Jpn.*, **23** (1983), 23.
20) M. Umemoto, I. Tamura and H. Otsuka: *Tetsu-to-Hagané*, **68** (1982), S1384.
21) T. Furuhara and T. Maki: Proc. of J. J. Jonas Symp. on Thermomechanical Processings of Steel, ed. by S. Yue and E. Essadipi, CIM, Montreal, Quebec, (2000), 465.
22) J. R. Yang and H. K. D. H. Bhadeshia: *Mater. Sci. Technol.*, **5** (1989), 93.
23) T. Furuhara, Y. Shimohara, K. Wada and T. Maki: *Tetsu-to-Hagané*, **80** (1994), 318.
24) M. Enomoto: *Z. Metallkd.*, **90** (1999), 19.
25) K. Hans, T. D. Mottishaw, G. D. W. Smith and D. V. Edmonds: *Mater. Sci. Technol.*, **10** (1994), 955.
26) D. Turnbull: Impurity and Imperfections, ASM International, Metals Park, Ohio, (1955), 121.
27) A. H. Cottrell: *Mater. Sci. Eng.*, **10** (1994), 22.
28) A. H. Cottrell: *Mater. Sci. Eng.*, **10** (1994), 788.
29) Z.-G. Yang and M. Enomoto: *Metall. Mater. Trans.*, **32A** (2001), 267.
30) S. Zhang, Y. Hattori, M. Enomoto and T. Tarui: *ISIJ Int.*, **36** (1996), 1301.
31) Z. G. Yang and M. Enomoto: *Mater. Sci. Eng.*, **A332** (2002), 184.
32) Y. Yazawa, T. Furuhara and T. Maki: *CAMP-ISIJ*, **12** (1999), 443.
33) M. Hillert and L.-I. Staffansson: *Acta Chem. Scand.*, **24** (1970), 3618.
34) R. Becker: *Ann. Phys.*, **32** (1938), 128.
35) J. H. van der Merwe and C. G. Ball: Epitaxial Growth, Academic Press, NY, (1975), 493.
36) T. Nishizawa: *Bull. Jpn. Inst. Met.*, **12** (1973), 401.
37) M. Hillert and L-I. Staffansson: *Mater. Trans. B*, **7B** (1976), 203.
38) W. Huang: *Z. Metallkd.*, **82** (1991), 391.
39) H. Ohtani and M. Hillert: *Calphad*, **15** (1991), 25.
40) G. Spanos: Ph. D thesis, Carnegie-Mellon University, (1989), 65.
41) W. Bollmann: Crystal Defects and Crystalline Interfaces, Springer-Verlag, New York, (1970), 143.
42) J. P. Hirth and J. Lothe: Theory of Dislocations, 2nd ed., Wiley-Interscience, NY, (1982), 740.
43) Z. Nishiyama: *Sci. Rep. Tohoku Imp. Univ.*, **25** (1936), 79.
44) G. Wassermann: *Arch. Eisenhüttwes.*, **16** (1933), 647.
45) N. Sugita: Master Thesis, Kyoto University, (1997).

Appendix I. Calculation of Chemical Component in Interphase Boundary Energy

Turnbull[26] proposed that the energy of the semi-coherent interphase boundary is approximately given as the sum of the chemical component (which originates from the difference in the type and the number of the bonds across the boundary) and the structural component (which originates from the self and interaction energy of misfit dislocations).

The chemical component of interfacial energy was calculated by counting the bonds broken and formed across the boundary, respectively. The bond energy of each pair was estimated from the interaction parameters in the HSM.[33] The partial molar Gibbs free energies in Fe–X–M ternary systems are given as follows (M: substitutional alloying element, X: interstitial alloying element, V: interstitial vacancy);

$$\begin{aligned} a\,{}^{\mathrm{E}}G_{\mathrm{Fe}} = & -Y_{\mathrm{M}}Y_{\mathrm{X}}\{\Delta G_{\mathrm{M}} + {}^{0}L_{\mathrm{X}}^{\mathrm{FeM}} - {}^{0}L_{\mathrm{V}}^{\mathrm{FeM}} + L_{\mathrm{M}}^{\mathrm{XV}} - L_{\mathrm{Fe}}^{\mathrm{XV}} \\ & + (1-2Y_{\mathrm{M}})({}^{1}L_{\mathrm{V}}^{\mathrm{FeM}} - {}^{1}L_{\mathrm{X}}^{\mathrm{FeM}})\} + Y_{\mathrm{M}}^{2}\{{}^{0}L_{\mathrm{V}}^{\mathrm{FeM}} - (3-4Y_{\mathrm{M}}) \\ & + L_{\mathrm{V}}^{\mathrm{FeM}}\} + Y_{\mathrm{X}}^{2}L_{\mathrm{Fe}}^{\mathrm{XV}} + 2Y_{\mathrm{M}}^{2}Y_{\mathrm{X}}\{{}^{0}L_{\mathrm{X}}^{\mathrm{FeM}} - {}^{0}L_{\mathrm{V}}^{\mathrm{FeM}} \\ & + (2-3Y_{\mathrm{M}})({}^{1}L_{\mathrm{V}}^{\mathrm{FeM}} - {}^{1}L_{\mathrm{X}}^{\mathrm{FeM}})\} + 2Y_{\mathrm{M}}Y_{\mathrm{X}}^{2}(L_{\mathrm{M}}^{\mathrm{XV}} - L_{\mathrm{Fe}}^{\mathrm{XV}}) \\ a\,{}^{\mathrm{E}}G_{\mathrm{M}} = & Y_{\mathrm{Fe}}Y_{\mathrm{X}}\{\Delta G_{\mathrm{M}} + {}^{0}L_{\mathrm{V}}^{\mathrm{FeM}} - {}^{0}L_{\mathrm{X}}^{\mathrm{FeM}} + L_{\mathrm{M}}^{\mathrm{XV}} - L_{\mathrm{Fe}}^{\mathrm{XV}} \\ & + (1-2Y_{\mathrm{M}})({}^{1}L_{\mathrm{V}}^{\mathrm{FeM}} - {}^{1}L_{\mathrm{X}}^{\mathrm{FeM}})\} \\ & + Y_{\mathrm{Fe}}^{2}\{{}^{0}L_{\mathrm{V}}^{\mathrm{FeM}} - (1-4Y_{\mathrm{M}}){}^{1}L_{\mathrm{V}}^{\mathrm{FeM}}\} + Y_{\mathrm{X}}^{2}L_{\mathrm{M}}^{\mathrm{XV}} \\ & + 2Y_{\mathrm{Fe}}Y_{\mathrm{X}}\{{}^{0}L_{\mathrm{X}}^{\mathrm{FeM}} - {}^{0}L_{\mathrm{V}}^{\mathrm{FeM}} + (1-3Y_{\mathrm{M}})({}^{1}L_{\mathrm{X}}^{\mathrm{FeM}} - {}^{1}L_{\mathrm{V}}^{\mathrm{FeM}})\} \\ & + 2Y_{\mathrm{Fe}}Y_{\mathrm{X}}^{2}\,(L_{\mathrm{Fe}}^{\mathrm{XV}} - L_{\mathrm{M}}^{\mathrm{XV}}) \\ c\,{}^{\mathrm{E}}G_{\mathrm{X}} = & -Y_{\mathrm{X}}^{2}L_{\mathrm{Fe}}^{\mathrm{XV}} + Y_{\mathrm{M}}\{\Delta G_{\mathrm{M}} + {}^{0}L_{\mathrm{X}}^{\mathrm{FeM}} - {}^{0}L_{\mathrm{V}}^{\mathrm{FeM}} + L_{\mathrm{M}}^{\mathrm{XV}} - L_{\mathrm{Fe}}^{\mathrm{XV}}) \\ & + 2Y_{\mathrm{M}}Y_{\mathrm{X}}(L_{\mathrm{Fe}}^{\mathrm{XV}} - L_{\mathrm{M}}^{\mathrm{XV}}) + Y_{\mathrm{M}}^{2}\{{}^{0}L_{\mathrm{V}}^{\mathrm{FeM}} - {}^{0}L_{\mathrm{X}}^{\mathrm{FeM}}) \end{aligned}$$

where $\Delta G_{\mathrm{M}} = {}^{0}G_{\mathrm{Fe}} + {}^{0}G_{\mathrm{MX}c/a} - {}^{0}G_{\mathrm{FeX}c/a} - {}^{0}G_{\mathrm{M}}$, $Y_{\mathrm{Fe}} = x_{\mathrm{Fe}}/(1-x_{\mathrm{X}})$, $Y_{\mathrm{M}} = x_{\mathrm{M}}/(1-x_{\mathrm{X}})$, $Y_{\mathrm{X}} = a/c\ x_{\mathrm{X}}/(1-x_{\mathrm{X}})$, $Y_{\mathrm{X}} = a/c\ x_{\mathrm{X}}/(1-x_{\mathrm{X}})$, $a=1$, and $c=1$ (for austenite) or 3 (for ferrite), x_{i}: the mole fraction of i-component.

Following to the nearest neighboring bonding model by Becker,[34] the chemical component of interphase boundary energy is expressed as follows;

$$\begin{aligned} \sigma_{\mathrm{chem}} = & n_{\mathrm{s}}^{\mathrm{M}}(-Z_{\mathrm{s}}^{\mathrm{M-X}}u_{\mathrm{MX}} + Z_{\mathrm{s}}^{\mathrm{M-M}}\Delta E_1) \\ & + n_{\mathrm{s}}^{\mathrm{X}}(-Z_{\mathrm{s}}^{\mathrm{X-M}}u_{\mathrm{FeX}} + Z_{\mathrm{s}}^{\mathrm{X-X}}u_{\mathrm{XX}}) \end{aligned}$$

where n_{s}^{i} is the number of i atoms on the boundary with an unit area, Z_{s}^{i-j} is the numbers of i–j bonds per atom crossing the boundary. u_{ij} is the enthalpy of i–j bond, and $\Delta E_1 = u_{\mathrm{FeM}} - (u_{\mathrm{MM}} + u_{\mathrm{FeFe}})/2$. Here, the bond energy in B1-type precipitate is taken to be the same as that in austenite or in ferrite as a first approximation.

Using the expression of the interaction parameter $\varepsilon_i^{(j)}$, we

can relate the parameters to the Bragg–Williams regular solution model.[36] For examples,

$$\varepsilon_M^{(M)}=(\partial \ln \gamma_M^{\gamma}/\partial x_M^{\gamma})=NZ_s^{M-M}\{u_{FeM}-(u_{FeFe}+u_{MM})/2\}/RT$$
$$=-(3^1L_V^{FeM}+{}^0L_V^{FeM})/RT$$
$$\varepsilon_M^{(X)}=(\partial \ln \gamma_M^{\gamma}/\partial x_X^{\gamma})=NZ_s^{M-X}(u_{MX}-u_{FeX})/RT$$
$$=(\Delta G_M+{}^0L_X^{FeM}-{}^0L_V^{FeM}+L_M^{XV}-L_{Fe}^{XV})/RT$$
$$\varepsilon_X^{(X)}=(\partial \ln \gamma_X^{\gamma}/\partial x_X^{\gamma})=(1+1/r)+2NZ_s^{X-X}u_{XX}/rRT$$
$$\begin{cases}=2-2L_{XV}{}^{Fe}/RT & \text{for austenite}\\ =4/3-2L_{XV}{}^{Fe}/9RT & \text{for ferrite}\end{cases}$$

The free energy of Fe–Mn–S ternary system is described in the regular solution model as follows[37]:

$$G_m=\sum x_i{}^0G_i+RT\sum x_i \ln x_i+1/2\sum x_i x_j \Omega_{ij}$$

where x_i and ${}^0G_i$ are the mole fraction and the free energy of i-element, respectively, and Ω_{ij} is the interaction parameter in the i–j binary system. Taking only nearest neighboring bonds in austenite (or ferrite) and MnS into account, the chemical component of $(001)_{MnS}//(001)_{Fe}$ interphase boundary per unit area is given by the following equation for both austenite and ferrite under the observed orientation relationship given in Appendix II;

$$\sigma_{chem}(MnS)=(8u_{FeMn}+8u_{FeS}-16u_{FeFe}-4u_{MnS})/a_{MnS}^2$$

With the interaction parameters and the energies of pure elements, the bond energies in the system can be calculated using the following relationships:

$${}^0G_i=NZ^{M-M}u_{ii}/2$$
$$\Omega_{ij}=NZ^{M-M}(u_{ij}-(u_{ii}+u_{jj})/2)$$

Finally, the chemical component of interphase boundary energy between B1-type precipitate (VC, VN and MnS) and austenite (or ferrite) of pure iron was estimated with the thermodynamic parameters determined in Fe–Mn–S,[37] Fe–V–C[38] and Fe–V–N[39] ternary systems. In **Table A1**, the numbers of various bonds per unit interfacial area are listed.

Appendix II. Calculation of Structural Component in Interphase Boundary Energy

The structural component was estimated by the following equations proposed by van der Merwe *et al.*[35]

$$\sigma_{strl}=(\mu c/4\pi^2)[1+\beta-(1+\beta^2)^{1/2}-\beta\ln\{2\beta(1+\beta^2)^{1/2}-2\beta\}]$$

where $\beta=2\pi\delta\lambda/\mu$, $\lambda=1/[\{(1-v_m)/\mu_m\}+(1-v_p)/\mu_p\}]$, $c=(a_m+a_p)/2$, $\delta=(a_p-a_m)/c$, v_i is the Poisson's ratio, μ_i is the shear modulus and a_i is the lattice parameter of i phase. The parameters used to calculate the structural component is listed in **Table A2**. This equation gives the boundary energy for the single set of parallel misfit dislocations. At least, two sets of misfit dislocations are necessary for the misfit accommodation on general boundaries. When the dislocation lines and the Burgers vector is perpendicular each other for two sets, there is no interaction between the dislocation segments of different sets. Thus, the total structural component should be given as the sum of the calculated value for each set, which is applicable to the boundary energy of $\{001\}_{\gamma}//\{001\}_{V(C,N)}$. However, for the other cases, such interaction needs to be calculated. Spanos[40] calculated misfit dislocation structure by O-lattice theory[41] and estimated of the structural component of the fcc/fcc semi-coherent boundary energy with the cube–cube orientation relationship for different boundary orientations by taking all the interaction energy into account.[42] For the calculation of $\{111\}_{\gamma}//\{111\}_{V(C,N)}$ boundary energy, the boundary energy of $\{001\}_{\gamma}//\{001\}_{V(C,N)}$ was multiplied by the anisotropy factor of $\sigma_{strl}\{111\}_{fcc}/\sigma_{strl}\{001\}_{fcc}=1.06$ found in his analysis.

In the calculation of ferrite/V(C,N) boundary energy, two orthogonal sets of edge dislocations were assumed for the $(001)_{\alpha}//(001)_{V(C,N)}$ boundary with B–N relationship and $(011)_{\alpha}//(111)_{V(C,N)}$ boundary with Nishiyama[43]–Wassermann[44] relationship. The directions of misfit strain taken are in the following;

$$[100]_{\alpha}//[110]_{V(C,N),}\ [010]_{\alpha}//[\bar{1}10]_{V(C,N)}\ \text{on}$$
$$(001)_{\alpha}//(001)_{V(C,N)}$$
$$[100]_{\alpha}//[110]_{V(C,N),}\ [010]_{\alpha}//[11\bar{2}]_{V(C,N)}\ \text{on}$$
$$(001)_{\alpha}//(111)_{V(C,N)}$$

In the calculation of Fe/MnS boundary energy, two orthogonal sets of edge dislocations were assumed for the $(001)_{\alpha}//(001)_{MnS}$ boundary with the cube–cube orientation relationship[45] and the $(001)_{\gamma}//(001)_{MnS}$ boundary with the cube-on-edge orientation relationship. The directions of misfit strain taken are in the following;

$$[100]_{\alpha}//[100]_{MnS,}\ [010]_{\alpha}//[010]_{MnS}\ \text{on}$$
$$(001)_{\alpha}//(001)_{MnS}$$
$$[100]_{\gamma}//[110]_{MnS,}\ [010]_{\gamma}//[\bar{1}10]_{MnS}\ \text{on}$$
$$(001)_{\gamma}//(001)_{MnS}$$

Table A1. The numbers of various bonds per unit interfacial area at boundaries (a: lattice parameter of B1-type precipitate at the boundary). M=Fe, V and Mn and X=C, N and S.

Interface	precipitate/matrix OR	Number of bond per unit area		
		M-M	M-X	X-X
VX(001)/γ	cube-cube	$8/a^2$	$4/a^2$	$8/a^2$
VX(111)/γ	cube-cube	$6.928/a^2$	$6.928/a^2$	$6.928/a^2$
VX(001)/α	B-N	$8/a^2$	$4/a^2$	$8/a^2$
VX(111)/α	N-W	$6.928/a^2$	$6.928/a^2$	$6.928/a^2$
MnS(001)/γ	cube-on-edge	$8/a^2$	$4/a^2$	$8/a^2$
MnS(001)/α	cube-cube	$8/a^2$	$4/a^2$	$8/a^2$

Table A2. The parameters used to calculate the structural component of interphase boundary energy.

Phase	Lattice parameter a (nm)	Poisson's ratio	Young's modulus (N/m^2)	Shear modulus (N/m^2)
VC	0.4192	0.3333	4.22×10^{11}	1.58×10^{11}
VN	0.4161	0.3333	4.22×10^{11}	1.58×10^{11}
MnS	0.5285	0.3333	3.00×10^{11}	1.58×10^{11}
γ	0.3673	0.3333	2.10×10^{11}	7.88×10^{10}
α	0.2896	0.3333	2.10×10^{11}	7.88×10^{10}